

# Optimization of a UV light-emitting diode based fluorescence-phase sensor

A. Žukauskas<sup>a</sup>, N. Kurilčik<sup>a</sup>, P. Vitta<sup>a</sup>, S. Juršėnas<sup>a</sup>, E. Bakienė<sup>b</sup>, R. Gaska<sup>c</sup>

<sup>a</sup>Institute of Materials Science and Applied Research, Vilnius University  
Saulėtekio al. 9, Building III, LT-10222 Vilnius, Lithuania

<sup>b</sup>Department of Biochemistry and Biophysics, Vilnius University  
M. K. Čiurlionio 21/27, LT-03101 Vilnius, Lithuania

<sup>c</sup>Sensor Electronic Technology, Inc., 1195 Atlas Road, Columbia, SC 29209 USA

## ABSTRACT

A set of UV light-emitting diodes (LEDs) with the peak wavelengths ranging from 255 nm to 375 nm was applied for the investigation of spectral and decay-time fluorescence signatures in dry *B. globigii* spores and common airborne interferants (albuminous, epithelium, and cellulosous materials as well as aromatic hydrocarbons). The fluorescence decay signature was represented by a phase shift of the sinusoidal fluorescence waveform in respect of excitation provided by high-frequency modulated LEDs. The obtained data matrix was used for the optimization a bioparticle fluorescence sensor with a minimized number of excitation sources and detection channels and maximized discrimination ability of bioparticles against common interferants. Based on the optimization, a new concept for a UV LED based “detect-to-warn” bioparticle fluorescence sensor is proposed. The sensor contains a single deep-UV LED emitting at 280 nm that is harmonically modulated at a high frequency (of about 70 MHz) and a dual-channel fluorescence detector with the spectral windows peaked at 320 nm and 450 nm. The output parameters of the sensor are the ratio of the fluorescence intensity in the two windows and the phase shift of the fluorescence waveform in the 320-nm detection channel in respect of the excitation one. Such a sensing scheme has a smaller number of optical components and a potentially higher discrimination ability of bioparticles against common interferants in comparison with the conventional approach based on just fluorescence intensity measurement under dual-wavelength excitation (280 nm and 340 nm).

**Keywords:** UV LEDs, fluorescence lifetime, frequency-domain measurements, bioparticle fluorescence sensor

## 1. INTRODUCTION

Due to an increased threat of biological attacks from military units sponsored by rouge political regimes and from uncontrolled terrorist groups, there is a need for compact, low-maintenance and inexpensive “detect-to-warn” sensors of aerosol bioparticles operating in real time. To that end, optical methods of bioparticle sensing are addressed with increasing interest.<sup>1</sup> Of those methods, fluorescence measurements are the most commonly used technique with the highest ratio of discrimination ability to cost. In particular, several directions in the development of fluorescence sensors evolved. One of the directions is based on a single particle interrogation, which requires highly collimated excitation beams provided exclusively by lasers. Another direction is based on accumulation of extended samples which allows for use of sources of incoherent light, namely LEDs. The latter approach offers considerably lower price and size of a sensor at some expense in discrimination ability. Insufficient discrimination ability is the main drawback of both approaches resulting in an inadmissibly high false alarm rate. In both cases, this drawback is somewhat mitigated in matured systems that contain means of preselection of particles within a particular range of sizes using elastic scattering of light. Nevertheless, for the development of highly reliable bioparticle sensor networks for detect-to-warn purposes, further improvement in discrimination ability of the fluorescence measurements is required.

To improve the discrimination ability, an additional dimension of fluorescence, decay-time characteristics, was introduced into the arsenal of bioparticle fluorescence sensing.<sup>2-4</sup> In particular, the fluorescence decay signature of

airborne particles can be extracted by simple real-time measurement of the phase shift between the sinusoidal waveform of a high-frequency modulated excitation source and the waveform of the fluorescence.<sup>5</sup> Such a technique can be implemented using both lasers and LEDs as excitation sources. Recently, we demonstrated discrimination of *B. globigii* spores against common interferants based on frequency-domain fluorescence phase measurements using UV LEDs.<sup>3</sup> Recent progress in the fabrication of deep-UV AlGaIn LEDs, which are currently commercially available in a wide range of peak wavelengths,<sup>6,7</sup> allow for the development of novel schemes of fluorescence sensing with a reduced number of optical components and with the discrimination ability improved due to the exploiting of the fluorescence-lifetime signatures.

A well-established concept of a bioparticle fluorescence sensor contain two excitation sources (xenon lamps, lasers, or LEDs) emitting in the range at about 280-nm and 340-nm and two or three optical detector channels with the optical filters that allow for fluorescence intensity measurement in the near-UV and blue-green regions, respectively.<sup>8-10</sup> However, there exists no viable concept of a bioparticle fluorescence sensor, which employs an additional detection channel for the characterization of fluorescence decay time. A straightforward introduction of such a channel can result in a significant increase in the sensor price. In particular, an increase in a number of detectors should be avoided, since sensitive photodetectors, such as photomultiplier tubes (PMTs), and components for optical routing and filtering of fluorescence are the principal contributors to the price of the sensor.

In this paper we present our work on the development of a concept of a LED-based bioparticle fluorescence-phase sensor with an optimal design. To optimize the sensor, we obtained a matrix of spectral and phase-shift data for fluorescence excited in *B. globigii* spores and in a number of common interferants (albuminous, epithelium, and cellulosous materials as well as aromatic hydrocarbons) using a set of commercially available UV LEDs with the peak wavelengths ranging from 255 nm to 375 nm. The analysis of the data matrix enabled us to develop a concept of the sensor with a minimized number of optical components. The sensor contains just a single excitation source (280-nm LED modulated at about 70 MHz frequency) and a conventional dual-channel optical detector with the optical windows at 320 nm and 450 nm. The 320-nm detector branch is proposed to simultaneously use for the fluorescence phase measurement. In comparison with a conventional dual-source–dual/triple-detector fluorescence sensor, our concept sensor has a potentially inexpensive additional electronic circuitry and a simplified optical assembly and offers an improved discrimination ability of airborne bioparticles against common aerosol interferants.

The structure of the paper is as follows. The experimental technique and materials investigated are described in Section 2. In Section 3, data matrix of the fluorescence spectral and lifetime signatures of *B. globigii* and common airborne interferants is discussed and summarized. In Section 4, the optimization goals are considered and a concept fluorescence-phase sensor is proposed. We conclude with a brief summary in Section 5.

## 2. EXPERIMENTAL

### 2.1. Measurement technique

Commercially available deep-UV AlGaIn LEDs, developed by Sensor Electronic Technology, Inc. (SETI, Columbia, SC, USA) and near-UV InGaIn LEDs developed by Nichia Corp. (Japan; purchased from Nichia Europe BV, Amsterdam, the Netherlands) were tested for the spectral purity of the emission and high-frequency modulation ability, the characteristics that are of crucial importance for fluorescence-spectra and frequency-domain fluorescence lifetime measurements. At a 20-mA driving current, the SETI deep-UV LEDs (specified for 255 nm, 270 nm, 280 nm, 300 nm, 320 nm, and 340 nm peak wavelengths) and Nichia near-UV LEDs (specified for 365 nm and 375 nm peak wavelengths) delivered from 0.4 to 2.5 mW and about 2 mW output power, respectively. High-contrast emission spectra were resolved using a calibrated low-stray-light double monochromator (JY HRD1) and recorded using a UV-enhanced photomultiplier operating in the photon counting mode (Hamamatsu R1463P). For the frequency-response measurements, the LEDs were driven using a bias tee (Picosecond 5547). The bias current was 20 mA and radio-frequency modulation of +5 dbm in the frequency range from 0.25 to 200 MHz was provided by a high-power digital signal generator (Aeroflex IFR 2023A). The optical signal was recorded by a 0.78-ns risetime photomultiplier (Hamamatsu H6780-01) and measured by a radio-frequency lock-in amplifier (Stanford Research Systems SR844).

Figure 1a shows the emission spectra within a dynamic range of over 5 orders of magnitude. The spectra peak at 258 nm, 271 nm, 282 nm, 298 nm, 315 nm, and 343 nm for the SETI LEDs and at 368 nm and 378 nm for the Nichia LEDs, respectively, and match the manufacturer's specification within 5-nm accuracy. The full width at half magnitude of the line is from 10 to 12 nm for the SETI LEDs and from 11 to 13 nm for the Nichia LEDs, respectively. The emission line is asymmetric and a long-wavelength wing ranging throughout the entire visible spectrum is observed. The highest intensity of the far long-wavelength background is seen to constitute about  $2 \times 10^{-4}$  of that at the main emission peak, whereas the typical background-to-peak ratio of the integrated intensities is in the range of  $10^{-3}$ . For high sensitivity measurements of biofluorescence, this ratio can be improved by using appropriate sets of mutually extinguishing optical filters (see below).

Figure 1b shows the modulation characteristics of the SETI and Nichia LEDs in the frequency range of 0.25–200 MHz. The SETI LEDs exhibit a pronounced modulated emission up to the frequency of 200 MHz. The cut-off frequencies are from 110 to 170 MHz for the SETI LEDs and about 20 MHz for the Nichia LEDs. The modulation ability for the SETI LEDs is sufficient for the measurement of phase shifts between the excitation and fluorescence waveforms for extraction of fluorescence decay time in the subnanosecond range relevant to the biofluorophore identification. Despite smaller cut-off frequencies, Nichia LEDs are also applicable for frequency-domain measurements of fluorescence lifetime in the same range with a lower sensitivity, however.

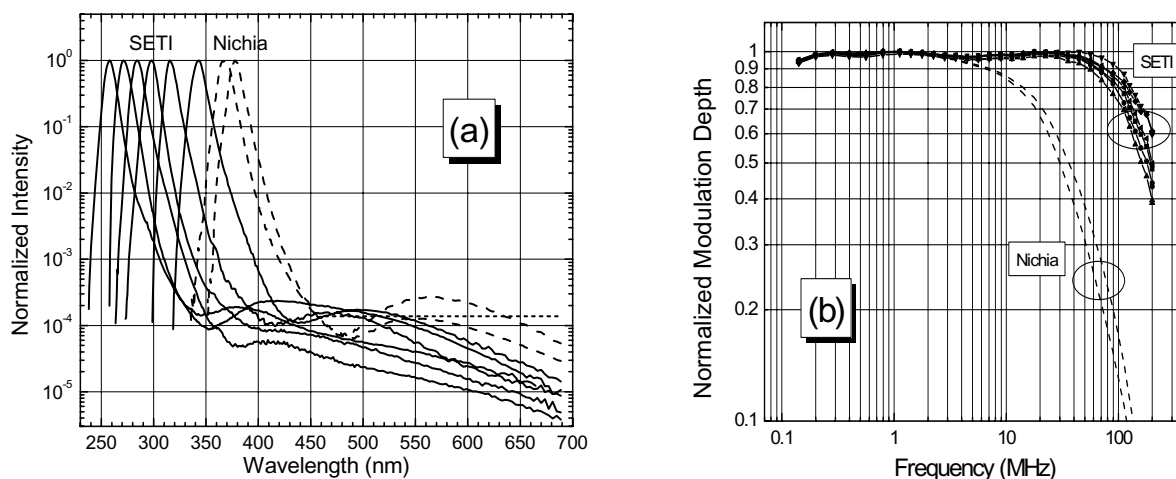


**Fig. 1.** (a) Electroluminescence spectra of the SETI UV LEDs with the peak wavelengths at 258 nm, 271 nm, 282 nm, 298 nm, 315 nm, and 343 nm (solid lines), and of the Nichia LEDs (368 nm and 378 nm, dashed lines). (b) Modulation characteristics of the SETI LEDs with the cut-off frequencies of 110-170 MHz (solid lines) and of the Nichia LEDs with the cut-off frequencies of about 20 MHz (dashed lines).

The set of eight LEDs characterized was used for excitation of fluorescence of *B. globigii* spores (stimulant of hazardous biological agent *B. anthracis*) and various autofluorophores and interferants. Fluorescence spectra were recorded using the same experiment setup as described above. In the frequency-domain fluorescence lifetime measurement setup, the modulated UV LED excitation was collimated, filtered by short-pass filter (SPF), reflected by a dichroic mirror and focused on a sample. The incident power was measured by a photodiode gauge (Ophir Nova/PD300-UV) with the detector head placed in the plane of the sample. Fluorescence from the sample was collimated by the same fused silica lens, passed through the dichroic mirror, filtered by a low-pass filter (LPF) and focused on the cathode of the photomultiplier. The electrical signal was split into ac and dc components by the bias tee and fed into the radio-frequency lock-in amplifier that measured the fluorescence phase and modulation depth.<sup>11</sup> The use of a harmonically modulated LED source for fluorescence excitation allows for the measurement of fluorescence lifetime by a simple comparison between the phase and modulation depth of the excitation and fluorescence signals.<sup>5</sup> More details of the experimental set-up and method used for frequency-domain fluorescence measurements are described in our previous papers.<sup>2,3</sup>

To optically isolate the excitation branch from the detection one, sets of mutually extinguishing SPFs and LPFs as well as dichroic filters were designed and assembled. In measurements using 255-nm, 270-nm, and 280-nm, LEDs, the excitation was passed through a custom-made interference filter with a cut-off wavelength of 290 nm and the dichroic mirror had the cut-off wavelength of 300 nm. The LPF was stacked of a custom made interference filter with a cut-off wavelength of 310 nm and either a Schott UG1 glass filter (2 mm thick) for the detection in the UV region (transmittance peak around 320 nm) or Schott color glasses GG420 (3 mm thick) and BG25 (4 mm thick) for the detection in the blue region (transmittance peak around 450 nm). In measurements using 300-nm, 320-nm, 340-nm, 365-nm, and 375-nm LEDs, a Schott UG11 glass filter stood for the SPF and the dichroic mirror had the cut-off wavelength of 390 nm. The LPF for the blue region was the same as for deep-UV excitation (GG420/BG25). All custom-made dichroic mirrors and interference filters were manufactured by Optida Ltd., Vilnius.

## 2.2 Biological materials and interferants

Spores of *B. globigii* (also, *B. antrophaeus*) ATCC 9372 (BAG-Biologische Analysen System GmbH, Germany) were prepared as described in Refs. 3, 12, and 13. Here we used dry spores subjected to multiple washing procedures in order to obtain fluorescence spectral and lifetime signatures as close to intrinsic ones as possible. (Basically, fluorescence in the blue-green part of the spectrum is known to be sensitive to the method of the spore preparation.<sup>14</sup>) Natural biofluorophores contained in bacterial spores such as aromatic amino acids (derivatives of tyrosine and tryptophan), coenzymes nicotinamide adenine dinucleotide (NADH) and riboflavin as well as dipicolinic acid (DPA) were used for the analysis of the fluorescence spectral and decay-time signatures of *B. globigii*.

Several groups of typical airborne interferants such as albuminous, epithelium, and cellulosous materials as well as aromatic hydrocarbons were investigated. Common albuminous interferants were represented by ovalbumin (stimulant of viral particles) and wheat flour (stimulant of high-protein-content food particles). Epithelium-originated interferants were imitated by elastin and collagen (proteins that are found in skin). Cellulosous interferants were represented by purified cotton, various kinds of paper that contain cellulose of different chemical treatment and age, and office dust extracted from the filter of an air conditioning system. Diesel fuels (both of winter and summer brands) stood for hydrocarbon interferants.

Analytical-grade chemicals were used: L-tyrosine and NADH (Carl Roth GmbH, Karlsruhe, Germany), N-acetyl-L-tryptophanamide (NATA), ovalbumin, collagen and elastin (Sigma-Aldrich, St. Louis, MO), riboflavin (Reanal, Budapest, Hungary), DPA (Sigma-Aldrich, Fluka, China). L-tyrosine, NATA, NADH and riboflavin were dissolved in phosphate buffer (50 mM, pH 7.2) and the prepared solutions had the molar concentration of about 400  $\mu$ M. Fluorescence measurements of ovalbumin, collagen, elastin and DPA were carried out using powdered forms.

Other interferants such as diesel fuels of several brands, wheat flour, several types of paper, cotton, office dust were obtained from utility sources and investigated in their natural form.

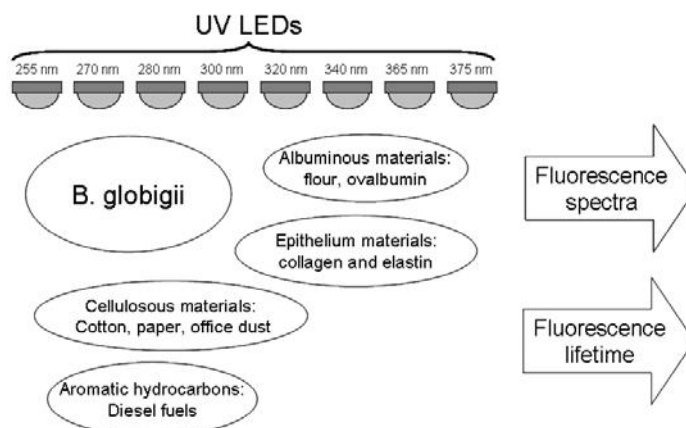
## 3. FLUORESCENCE DATA

### 3.1. Data matrix

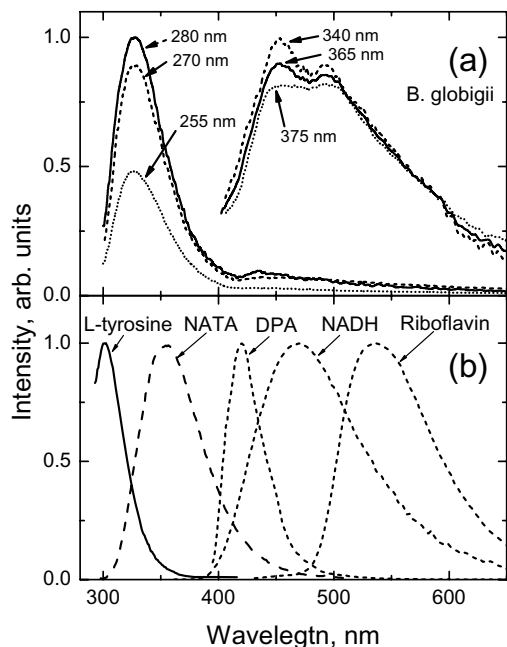
Figure 2 shows the general diagram of the acquisition of the fluorescence data matrix. UV LEDs of eight different emission wavelengths specified above were individually applied to excite fluorescence in *B. globigii* spores and in four groups of common interferants. Eventually for each type of LED, a set of fluorescence spectra was recorded and a set of fluorescence phase shift vs. frequency dependences was obtained. For deep-UV LEDs (255–280 nm), these dependences were measured for two spectral windows (peaked at 320 nm and 450 nm), whereas for the rest LEDs (300–375 nm) only the blue window (450 nm) was employed.

Figure 3 shows typical fluorescence spectra of *B. globigii* (a) and natural autofluorophores contained in spores (b) under excitation using LEDs with different peak wavelengths. Under 255-nm, 270-nm, and 280-nm excitation, fluorescence spectra of *B. globigii* are dominated by a band peaked at 325 nm (Fig. 3a, left). This near-UV band is due to protein amino acids, tyrosine and tryptophan. Although the peak position of the near-UV band is very close to that of unbound tyrosine in aqueous solution (Fig. 3b), the observed fluorescence is probably dominated by the tryptophan emission. This is a common situation in biological objects where the tyrosine emission is usually quenched by the energy transfer

to tryptophan,<sup>5</sup> whereas the tryptophan emission in nonpolar environment inside the protein globule displays a blue shift.<sup>15</sup> Also under deep-UV (255–280 nm) excitation, a weak band at about 440 nm can be resolved. Under excitation using the 300-nm LED, only the long-wavelength wing of the near-UV band can be observed, whereas for the 320-nm LED, this band is completely overlapped by the excitation line (these spectra are not shown in Fig. 3a). Under 340-nm, 365-nm, and 375-nm excitation, two bands peaked at about 450 nm and 500 nm can be resolved in the fluorescence spectra of *B. globigii* spores (Fig. 3a, right). These bands in the blue-green region can be attributed to fluorescence of DPA, NADH, and flavins, and (Fig. 3b).<sup>5,8,9,14,16–18</sup> Since the peaks observed in the *B. globigii* spectra can be shifted in respect of those observed in unbound fluorophores due to an inhomogeneous environment, it is difficult to unambiguously assign the blue-green emission to particular autofluorophores. Nevertheless, the most probable assignment is that the blue band in *B. globigii* is mainly due to DPA and NADH, whereas the green band is due to flavins.



**Fig. 2.** General diagram of the acquisition of fluorescence data matrix. Eight types of LEDs were used for excitation of fluorescence in *B. globigii* spores and common airborne intererents. The output of the experiment is the fluorescence spectra and fluorescence lifetime (represented by fluorescence phase shift in respect of the excitation waveform).



**Fig. 3.** (a) Fluorescence spectra of *B. globigii* spores under excitation using LEDs with different peak wavelengths (indicated). The intensities of the spectra in the two groups (255 nm/270 nm/280 nm and 340 nm/365 nm/375 nm) are normalized to the incident power. (b) Normalized fluorescence spectra of L-tyrosine and NATA (280-nm excitation) and DPA, NADH, and riboflavin (365-nm excitation).

Figure 4 shows some typical results of the fluorescence phase shift under 280-nm excitation measured within the 320-nm spectral window and under 365-nm excitation measured in the 450-nm spectral window. (Under 280-nm excitation, the signal in the 450-nm spectral window for most of the materials investigated was weak and a high accuracy was difficult to attain.) Both under 280-nm and 365-nm excitation, *B. globigii* spores exhibit phase shift vs. frequency dependences that reveal two-exponent fluorescence decay with the lifetimes in the subnanosecond and nanosecond range (Fig. 4a). Bacterial autofluorophores have single-exponent decay patterns,<sup>19</sup> except DPA, which exhibits a two-exponent decay (Fig. 4b). Since under 280-nm excitation the dependence for *B. globigii* was obtained within the 320-nm spectral window, both the short (0.89 ns) and the long (3.6 ns) components of the fluorescence lifetime are to be attributed to tryptophan in two different environments.<sup>5,20</sup> Under 365-nm excitation, the shorter component of the lifetime in *B. globigii* (0.60 ns) is probably contributed by NADH or the shorter component of DPA, whereas the longer component of *B. globigii* (7.9 ns) is probably due to flavins and the longer component of DPA.<sup>5,16,18</sup>

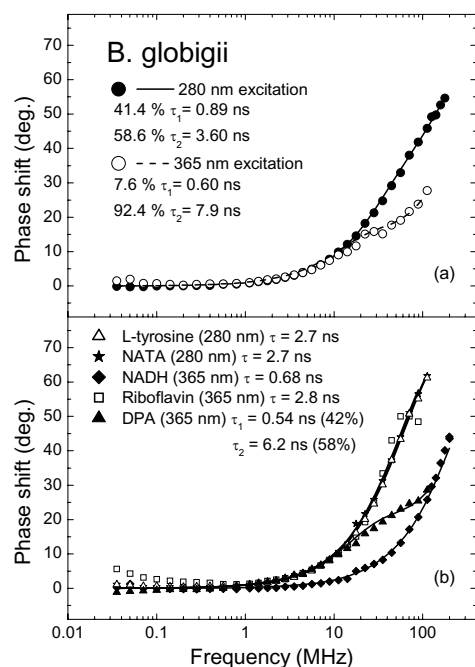


**Fig. 4.** Dependences of fluorescence phase vs. modulation frequency in *B. globigii* spores (a) under 280-nm (filled points) and 365-nm (open points) excitation and in bacterial autofluorophores (b) L-tyrosine (open triangles) and NATA (stars) under 280-nm excitation; NADH (diamonds), riboflavine (squares), and DPA (filled triangles) under 365-nm excitation. Data for 280-nm and 365-nm excitation was obtained within 320-nm and 450-nm spectral windows, respectively. Points, experiment; lines, the least-squares fit to single-exponent (L-tyrosine, NATA, NADH, and riboflavin) and two-exponent (*B. globigii* and DPA) fluorescence decay.

Below we discuss a part of the obtained fluorescence data matrix for two most important excitation wavelengths, 280 nm and 365 nm. The selection of these wavelengths was based on the following considerations. Three deep-UV LEDs with the wavelengths of 255 nm, 270 nm, and 280 nm, which match the spectral region of protein absorption, yielded almost identical results both in spectral and phase-shift characterization of *B. globigii* spores and the interferants. Of those three LEDs, the 280-nm one excites near-UV fluorescence in the spores with the highest efficiency. Also under 280-nm excitation, fluorescence in the blue region has somewhat higher relative intensity than under 255-nm and 270-nm excitation. Therefore, the 280-nm excitation wavelength was selected as the most appropriate one for further discussion in more detail.

The 300-nm and 320-nm LEDs were ruled out because of difficulties in isolation of excitation and fluorescence in the near-UV region and a low intensity of the excited fluorescence in the blue region. All three rest LEDs (340 nm, 365 nm, and 375 nm) are suitable for excitation of fluorescent coenzymes. These three excitation wavelengths resulted in almost identical fluorescence phase shifts. However, with increasing excitation wavelength in the 340-375 nm range, the peak intensity of the blue band somewhat decreases, whereas the relative contribution of the green band increases (Fig. 3a). Based on the trade-off between the overall fluorescence intensity and green to blue fluorescence intensity ratio, which is related to the informativeness of the spectra, the 365-nm LED was selected for the further discussion as the most appropriate one.

Figure 5 shows fluorescence spectra (a to d) and phase dependences (e and f) of *B. globigii* spores vs. cellulosous materials (typical paper, pure cotton, and office dust) under 280-nm (solid lines) and 365-nm (dashed lines) LED excitations. As discussed above, fluorescence spectra of *B. globigii* (Fig. 5a, which contain same data as Fig. 3a) reveal that under 280-nm excitation *B. globigii* spores exhibit an intense peak in the near-UV region (around 325 nm) due to tryptophan and a rather weak emission in the blue-green region. It is to be noted that a high ratio of near-UV to blue-green emission is typical of highly washed spores and can be much smaller in spores that are less refined (see e.g. our previous paper<sup>3</sup>). A typical characteristic of fluorescence spectra of the cellulosous materials (Figs. 5b to d) is a broad band peaked in the blue region (around 440 nm) with extended wings in both UV and green regions.<sup>21</sup> Although different cellulosous materials exhibit different ratios of the blue to near-UV and blue to green intensities, basically the near-UV and green wings are always weaker in intensity than the blue peak. For 365-nm LED excitation, two peaks in the fluorescence spectra of *B. globigii* spores can be clearly resolved (at about 450 nm and 500 nm), whereas the cellulosous materials show broad bands in the same blue-green region. Obviously, the blue-green emission of the spores is difficult to distinguish from that of the cellulosous materials, especially by low spectral resolution detectors used in inexpensive fluorescence sensors.

Figures 5e and f show the results of the measurement of the fluorescence phase in *B. globigii* spores vs. the cellulosous materials. For 280-nm excitation (Fig. 5e), such substances as paper and office dust exhibit much smaller phase shifts, i.e. smaller fluorescence decay times, than the spores. Pure cotton has higher values of the phase shift, but still below that of the spores. For 365-nm excitation (Fig. 5d), the phase vs. frequency dependence of *B. globigii* spores overlaps with those of the cellulosous materials and no discrimination can be performed.

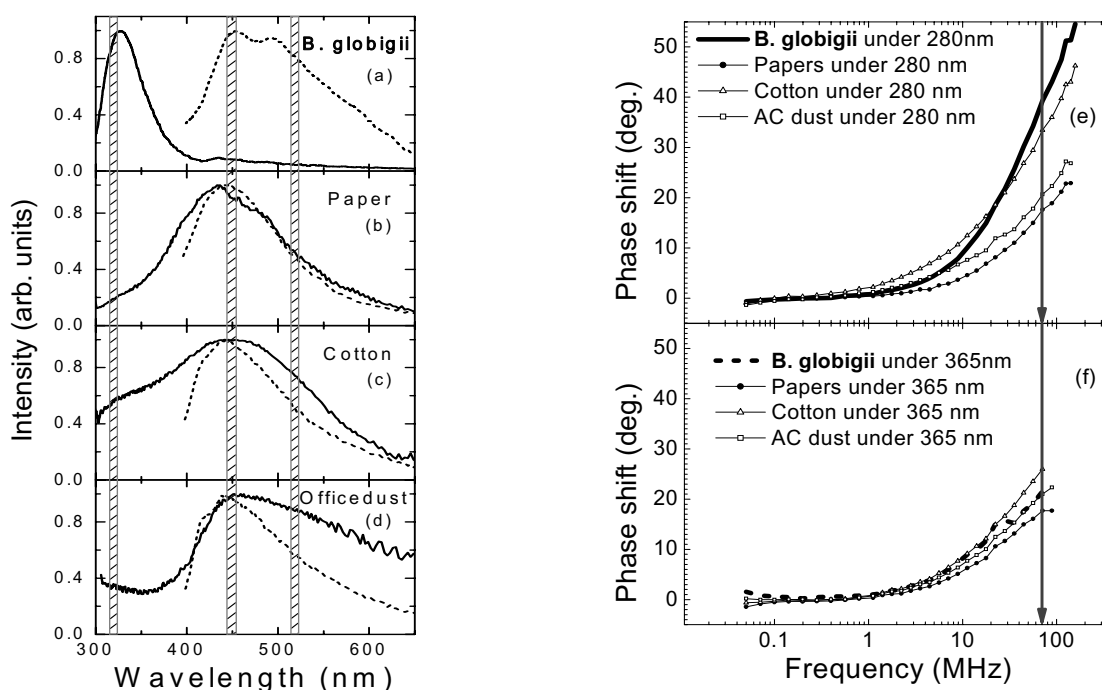


**Fig. 5.** Fluorescence spectra of *B. globigii* spores (a) vs. cellulosous materials paper (b), cotton (c) and AC dust (d) under 280-nm (solid line) and 365-nm (dashed line) excitation. Phase shift under 280-nm (e) and 365-nm (f) excitation as a function of frequency for *B. globigii* spores (solid line for 280-nm excitation, dashed line for 365-nm excitation), paper (filled circles), cotton (opened triangles) and AC dust (opened squares).

Fluorescence spectra of *B. globigii* spores are compared with those of the epithelium materials in Fig. 6a to c. Under 280-nm excitation (solid lines), both elastin (Fig. 6b) and collagen (Fig. 6c) have intense features in the near-UV region (around 310 nm), probably due to tryptophan in the environment somewhat different from that in the spores.<sup>5,20</sup> In the blue region, these compounds exhibit a broad band that is much more intense than the blue one in the washed spores.

Under 365-nm excitation (dashed lines), the epithelium materials show an intense band in the blue region (around 440 nm) with a broad wing extending in to the green region.<sup>18</sup> Although the blue-to-green fluorescence intensity ratio is somewhat higher in the epithelium materials than in the washed spores, this ratio is difficult to exploit as a reliable discrimination parameter taking into account the sensitivity of the fluorescence spectra of the spores to the preparation conditions.

Comparison of the fluorescence phase in the spores with that in the epithelium materials reveals a strong overlap under 280-nm excitation (Fig. 6d) despite different environments of tryptophan. Our data matrix shows that this overlap can be partially mitigated with shifting of the excitation to shorter wavelengths (e.g., 255 nm), however no high discrimination can still be achieved. Contrarily, under 365-nm excitation, the epithelium materials show much larger phase shifts in comparison with those in the spores. We attribute such a difference to a completely different origin of the blue emission in collagen and elastin, which is due to pyridinoline groups.<sup>22</sup>

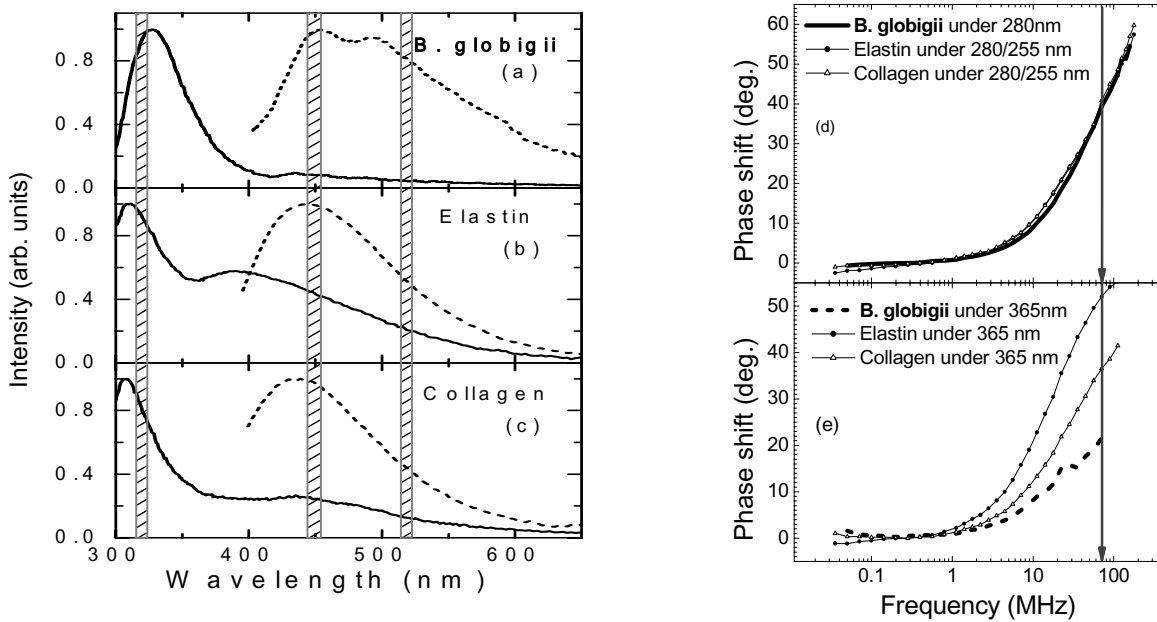


**Fig. 6.** Fluorescence spectra of *B. globigii* spores (a) vs. epithelium materials elastin (b) and collagen(c) under 280-nm (solid line) and 365-nm (dashed line) excitation. Phase shift under 280-nm (d) and 365-nm excitation as a function of frequency for *B. globigii* spores (solid line for 280-nm excitation, dashed line for 365-nm excitation), elastin (filled circles) and collagen (opened triangles).

Figures 7a to c show fluorescence spectra of *B. globigii* vs. albuminous materials. Under 280-nm excitation (solid lines), both ovalbumin (Fig. 7b) and flour (Fig. 7c) exhibit fluorescence spectra with an intense peak at about 330 nm. These spectra are dominated by emission of protein<sup>5,20</sup> and are very similar to that of the spores (Fig. 7a). Under 365-nm excitation (dashed lines), the albuminous materials feature a single blue band peaked at about 440 nm. Due to the absence of a green band, the blue-to-green intensity ratio is somewhat lower than in the spores, however we suggest that these differences are too small to provide with reliable discrimination in low spectral resolution sensors.

Figure 7d and e show the results on the fluorescence phase shift measurements for the two excitation wavelengths. Under 280-nm excitation (Fig. 7d), lower phase shifts for *B. globigii* spores can be clearly resolved in comparison with ovalalbumin and flour. Under 365-nm excitation, such a difference in phase shifts can be even higher.

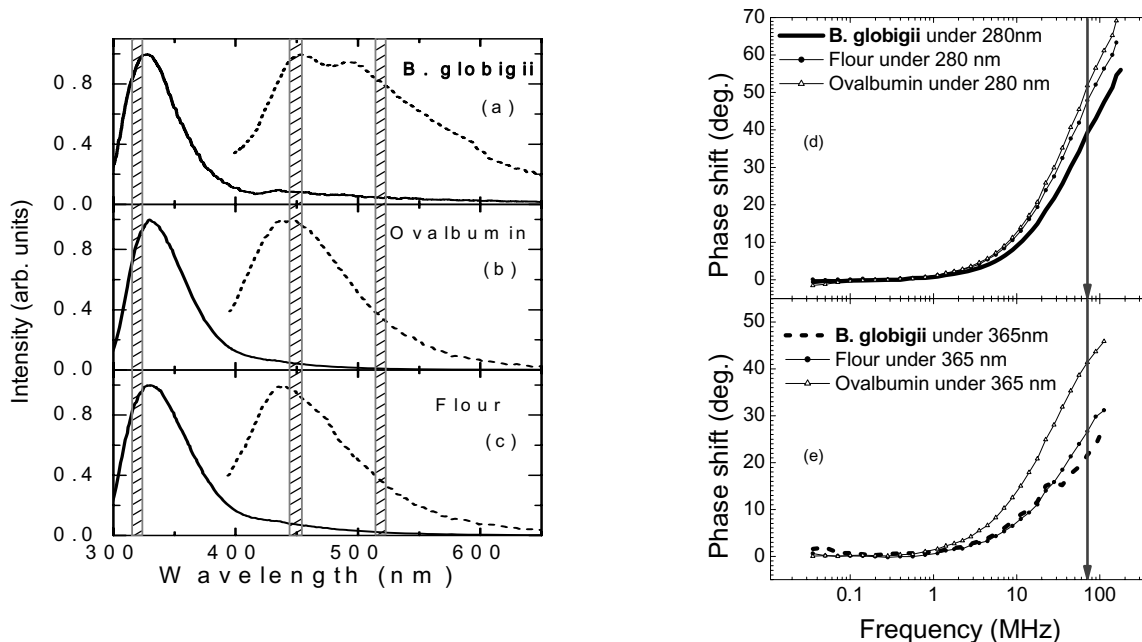


**Fig. 7.** Fluorescence spectra of *B. globigii* (a) vs. albuminous materials ovalbumin (b) and flour (c) under 280-nm (solid line) and 365-nm (dashed line) excitation. Phase shift under 280-nm (d) and under 365-nm (e) excitation as a function of frequency for *B. globigii* (solid line for 280-nm excitation, dashed line for 365-nm excitation), ovalbumin (opened triangles) and flour (filled circles).

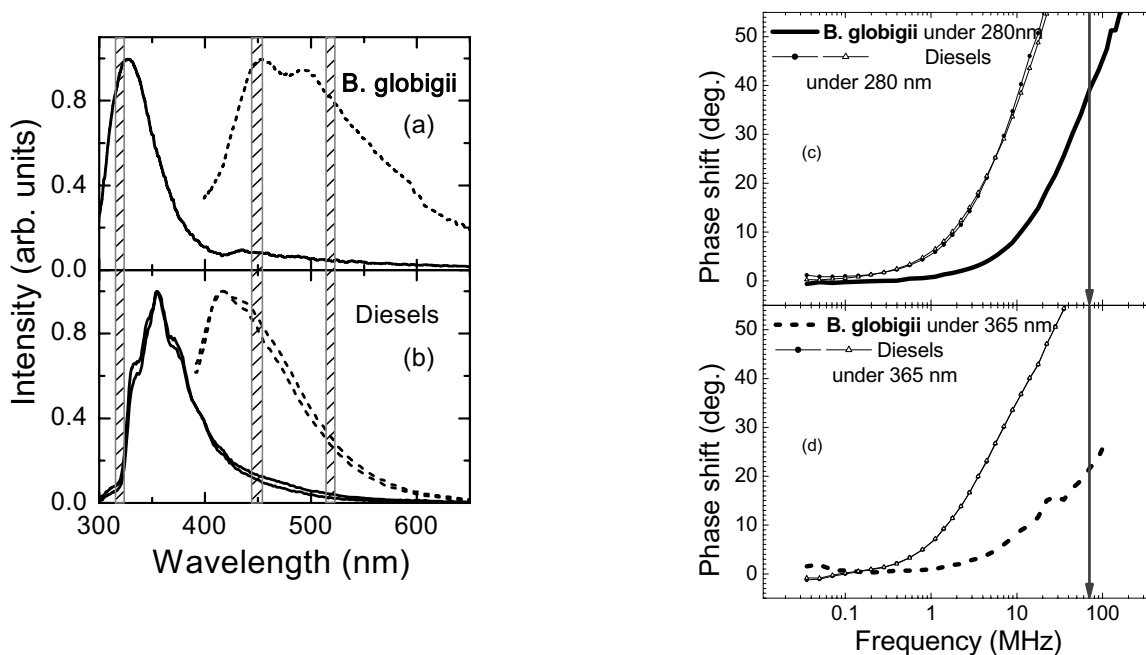


**Fig. 8.** Fluorescence spectra of *B. globigii* (a) vs. two kinds of diesel fuel materials (b) under 280-nm (solid line) and 365-nm (dashed line) excitations. Phase shift under 280-nm (c) and 365-nm (d) excitation as a function of frequency for *B. globigii* (solid line for 280-nm excitation, dashed line for 365-nm excitation) and two kinds of diesels (filled circles and opened triangles).

Figures 8a and b show fluorescence spectra of *B. globigii* spores vs. diesel fuels under 280-nm (solid lines) and 365-nm (dashed lines) excitation. For 280-nm excitation, the fluorescence spectra of diesel fuels (Fig. 8b) have a well-resolved band peaked at about 355 nm with an extended long-wavelength wing. Since this band, which is due to aromatic rings of hydrocarbons,<sup>23</sup> is shifted to longer wavelengths in comparison to the tryptophan band (Fig. 8a), the near-UV to blue intensity ratio is much lower than that for the spores. This difference in the near-UV to blue intensity ratio can be somewhat smaller in sensors with a low spectral resolution because of the proximity of the 355-nm band to the center of the 320-nm window, however. Fluorescence spectra of diesels under 365-nm LED excitation feature a band at about 420 nm. Again, the blue-to green intensity ratio is quite different from that of *B. globigii* spores and can be used for discrimination.

Figures 8c and d show the results of the fluorescence phase shift measurements for 280-nm and 365-nm excitation, respectively. In both cases, diesel fuels exhibit much larger phase shifts in comparison with those of the spores.

### 3.2. Discrimination charts

To design an optimal sensor, a set of the output parameters should be carefully selected to allow for high discrimination ability and reproducibility. Our selection of the set of output parameters was based on the following conditions. First, parameters, which combine data acquired using different excitation sources must be avoided because of different thermal drift and aging rate of the sources. Second, spectral signatures based on absolute fluorescence signals are inappropriate, since the detected intensity of the fluorescence signal depends on the size and number of the interrogated particles, contamination and ageing of the optical components, and drift of output of the excitation sources. Contrarily, fluorescence-phase signatures, which are almost independent on the excitation power and sensitivity of the detector, can be employed as absolute quantities. Consequently, the sets of the output parameters were built individually for each excitation source; they contain ratios of the fluorescence intensities and absolute values of the phase shifts.

Of eight excitation wavelengths used for the generation of the data matrix of the fluorescence spectral and phase signatures, two excitation wavelengths, 280 nm and 365 nm, were selected as yielding the most discriminative data (see sec. 3.1). Basing on the spectral peaks averaged over all materials investigated, fluorescence intensity in three spectral regions, around 320 nm, 450 nm, and 520 nm (shown by dashed areas in Figs. 5 to 8), were selected for use in the sensor output parameters. For the 280-nm LED, the corresponding output parameter was chosen as the ratio of fluorescence intensities at 320 nm and 450 nm, whereas for the 365-nm LED, the 450 nm to 520 nm intensity ratio was employed. Since these ratios vary within many orders of magnitude within the entire data matrix, a logarithmic presentation was used.

For the fluorescence decay signature, a single value of the fluorescence waveform phase shift in respect of the excitation one at a particular frequency and within a particular spectral window is sufficient to use as output parameter. Ideally, the most appropriate frequency for the highest discrimination of *B. globigii* against other fluorescent objects is that where the derivative of the phase shift vs. frequency dependence has the highest value, i.e. about 100 MHz where the phase shift is about 45 degrees (see Fig. 4a). However, because of many practical reasons (drop in the modulation ability of the LEDs, reduction of fluorescence modulation depth, and increase in parasitic electric crosstalk between the excitation and detection arms with frequency), a somewhat lower frequency is preferable. As a compromise, the frequency around 70 MHz was selected (vertical arrows in Figs. 5 to 8). For the 365-nm LED, the phase shift in the spectral window at 450 nm was employed, whereas for the 280-nm LED, of two possible spectral windows, only that at 320 nm was used. (As mentioned above, some materials under 280-nm excitation exhibit low fluorescence intensity in the 450-nm spectral window making measurements of the phase shift less accurate.)

Eventually, two-dimensional fluorescence discrimination charts were built for each of two excitation LEDs. Figure 8a shows the chart for the 280-nm LED with logarithm of the ratio of the fluorescence intensities at 320 nm and 450 nm standing for one coordinate and the phase shift at 71.8 MHz within the 320-nm spectral window standing for the second coordinate. Correspondingly, Fig. 8b shows the chart for the 365-nm LED. Here the horizontal coordinate is logarithm of the ratio of the fluorescence intensities at 450 nm and 520 nm, whereas the vertical coordinate is the phase shift at the same frequency within the 450-nm spectral window. Both charts are presented in the same scaling in order one could visually compare the discrimination ability for each excitation LED used. Fig. 8 clearly indicates that the ability of spectral discrimination of *B. globigii* spores against common interferants is much higher for excitation using the 280-nm

LED than for the 365-nm one (*cf.* the span of the data along the horizontal axis in Figs. 8a and 8b). Also, the deep-UV LED shows somewhat higher span of the data along the vertical axis, i.e. discrimination in the fluorescence phase shift.

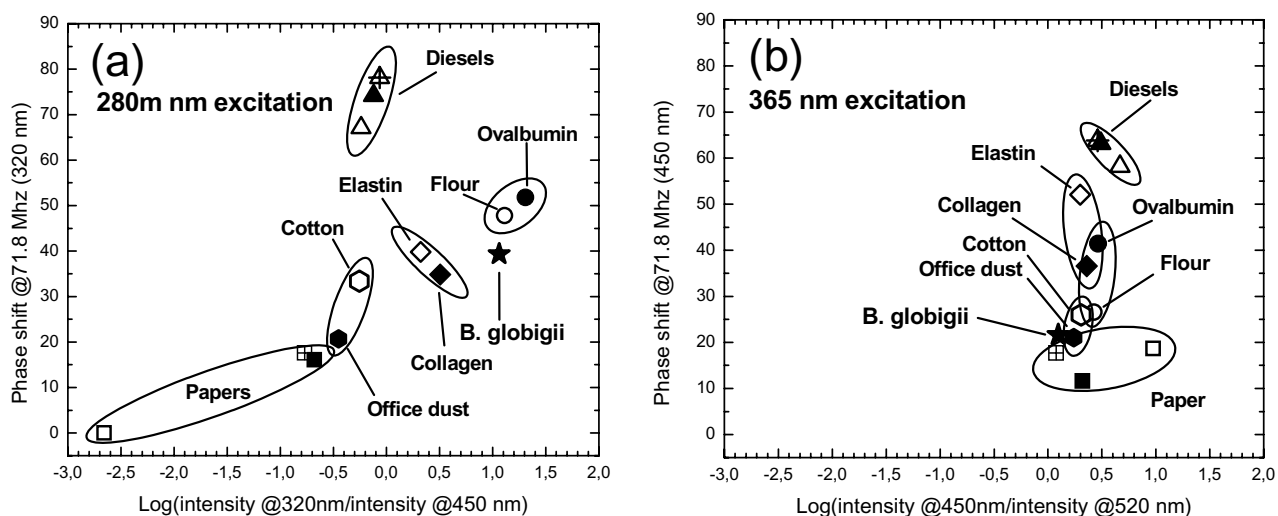


**Fig. 9.** (a) Distribution the fluorescence phase shift at 71.8 MHz vs. fluorescence intensity ratio at 320 nm and 450 nm for 280 nm excitation (a) and vs. fluorescence intensity ratio at 450 nm and 520 nm for 365-nm excitation (b).

To assess the applicability of the fluorescence spectral and phase signatures for use in a bioparticle sensor, we performed rating of the distances between the points corresponding to *B. globigii* and those nearest corresponding to various groups of interferants in Figs. 9a and 9b. Based on the reproducibility of the measurement data for *B. globigii* samples, differences in phase shift between 5 and 10 degrees were rated as rendering “moderate” discrimination, whereas those above 10 degrees were rated for “high” discrimination. Accordingly, differences in the fluorescence intensity ratio between 2 and 5 times were rated as rendering “moderate” discrimination, whereas those exceeding 5 times were rated for “high” discrimination. Table 1 presents the summary of the ratings for the two excitation wavelengths (280 nm and 365 nm).

**Table 1.** Ratings of fluorescence spectral and phase signatures in discrimination of *B. globigii* spores against various groups of interferants for excitation using 280-nm and 365-nm LEDs.

	UV to blue intensity, 280 nm LED	UV phase, 280 nm LED	Blue to green intensity, 365 nm LED	Blue phase, 365 nm LED
<i>B. globigii</i> vs. cellulosous materials	high	moderate	low	low
<i>B. globigii</i> vs. epithelium materials	moderate	low	low	high
<i>B. globigii</i> vs. albuminous materials	low	moderate	low	moderate
<i>B. globigii</i> vs. diesel fuels	high	high	moderate	high

#### 4. CONCEPT FLUORESCENCE-PHASE SENSOR

Discrimination charts (Figs. 9a and b) and summary presented in Table 1 were used for designing of an optimal scheme of a “detect-to-warn” bioparticle sensor. The main optimization objectives we posed were as follows i) use as few excitation sources as possible; ii) use as few optical detection channels as possible; iii) achieve high discrimination ability against common interferants; iv) operate in real time.

*Excitation sources.* Table 1 shows that when both the spectral and phase-shift signatures are employed for discrimination of *B. globigii* against common interferants, 280-nm excitation exhibits at least one high or moderate rating for albuminous, epithelium and cellulosous interferants and both high ratings for aromatic hydrocarbons. For 365-nm excitation, discrimination against epithelium materials is somewhat higher (low and high ratings vs. moderate and low), whereas both ratings for cellulosous materials are low. This suggests that when the fluorescence spectral signature is complemented by the decay-time signature (phase shift), a single 280-nm excitation source is stringent and almost sufficient for excitation. Alternatively, Table 1 implies that at least one high or moderate discrimination rating for each group of interferants can be obtained in a measurement scheme based solely on fluorescence intensity ratios when two excitation sources (280 and 365 nm) and three detection channels (320 nm, 450 nm, and 520 nm) are used. However, a single-source approach has many advantages in respect of the conventional two-source (280/340 nm) scheme. First, the number of expensive optical elements for filtering and routing excitation and fluorescence can be reduced and substituted by potentially cheap electronic circuits for the LED modulation and fluorescence phase measurement. Second, use of a single source requires no sharing of measurement time and switching between the detection arms activated by different sources what simplifies the electronics and reduces the reaction time of the sensor. Third, issues due to different thermal and ageing drift of different sources (e.g., normalization procedures) are avoided.

*Detection channels.* For 280-nm excitation, the 320-nm spectral window is the most appropriate for fluorescence-phase discrimination of bacterial spores against most interferants. However, the phase-shift signature is insufficient for high discrimination against some interferants and must be supplemented by a spectral signature. The latter requires at least two detection channels. Of those, one can employ the same 320-nm window, whereas the most appropriate second spectral window lies in the blue region (around 450 nm). Therefore in a sensor with fluorescence-phase measurement employed, two optical detection channels are sufficient. Meanwhile in a high-performance fluorescent sensor based solely on fluorescence intensity ratios, at least three optical detection channels are required.<sup>10</sup>

*Discrimination ability.* Obviously for the same number of the excitation sources and optical detection channels, a sensor with fluorescence phase measurement should be superior in discrimination ability to a conventional one based solely on the measurement of fluorescence intensity owing to a larger number of the output parameters. Even more, the above considerations imply that a fluorescence-phase sensor with a reduced number of the excitation sources and optical detection channels has somewhat higher overall discrimination ability in comparison to a conventional sensor (3 high, 3 moderate, and 2 low ratings vs. 2 high, 2 moderate, and 4 low ratings). Actually, replacement of the green to blue fluorescence spectral signatures provided by the near-UV excitation source (340–365 nm) by a fluorescence-decay signature provided by the deep-UV excitation source (255–280 nm) results in an improvement in discrimination, especially between the particles that contain proteins and those that do not. The reason is in that protein emission in the 320-nm range is dominated by a single amino acid, tryptophan, with the fluorescence lifetime specific to local environment. Meanwhile spectral signatures in the blue-green spectral region are sensitive to the purity of bacterial agents and are difficult to distinguish, especially when a bacterial agent is masked by interferants in particle mixtures that are usually interrogated in inexpensive LED-based sensors.

*Real time operation.* Basically, fluorescence lifetime signature can be obtained in either time domain (pulsed excitation) or frequency domain (harmonically modulated excitation). Both of two modes have advantages and disadvantages in respect of each other.<sup>5</sup> For research applications, the advantage of time-domain measurement is the direct acquisition of the temporal decay profile, which is very convenient, rather than of a phase vs. frequency dependence, which is a Fourier transform of the time dependence. Fortunately, for sensor applications this is not important, since both the decay time and phase shift are interconvertible unique signatures of a fluorophore. However for a sensor operating in real time, the frequency domain mode is more appropriate, since the measurement can be continuous without a need of separate stages of data accumulation and processing as in the time-domain mode. Also in the frequency-domain measurement mode, the fluorescence intensity and phase can be independently measured at the same time within one detection channel by simple branching of the dc and ac components of the photocurrent. Finally in the time domain mode, pulsed excitation requires high peak power that can result in artifacts due to the optical damage of the sample. These considerations infer that for real-time operation, use of the frequency-domain mode is preferable. However, further development of the frequency-domain technique is needed to catch up with the pulsed methods in terms of sensitivity. In particular, a method of phase shift measurement in the photon counting mode analogous to the time-correlated photon counting, which is widely used in the time-domain fluorescence lifetime measurements, is to be developed.

A simple scheme of a concept bioparticle sensor, which utilizes the fluorescence decay time signature, is presented in Fig. 10. The sensor contains a single excitation source, 280-nm LED that is modulated at a frequency of about 70 MHz using a harmonic oscillator. The emission of the LED is filtered by a SPF to improve the spectral purity. A sample accumulation unit is to be used to preselect airborne particles within a particular range of sizes using elastic scattering of light and to collect them on a non-fluorescent substrate. Fluorescence is detected in two channels that are equipped with LPFs designed for the 320-nm and 450-nm spectral windows, respectively. In the 450-nm channel, the photodetector (PMT) is used just for the fluorescence intensity measurement, whereas in the 320-nm channel the photocurrent is split in to the dc and ac components that are used for the measurement of the fluorescence intensity and phase, respectively. Two logarithmic amplifiers and a subtractor are used to output the ratio of the intensities and a phase meter provides with a signal related to the phase difference between the waveforms of the driving oscillator and fluorescence in the 320-nm channel. The sensor operates in a continuous regime and alarms when the two output signals synchronously fall within the ranges specific for a hazardous biological agent.

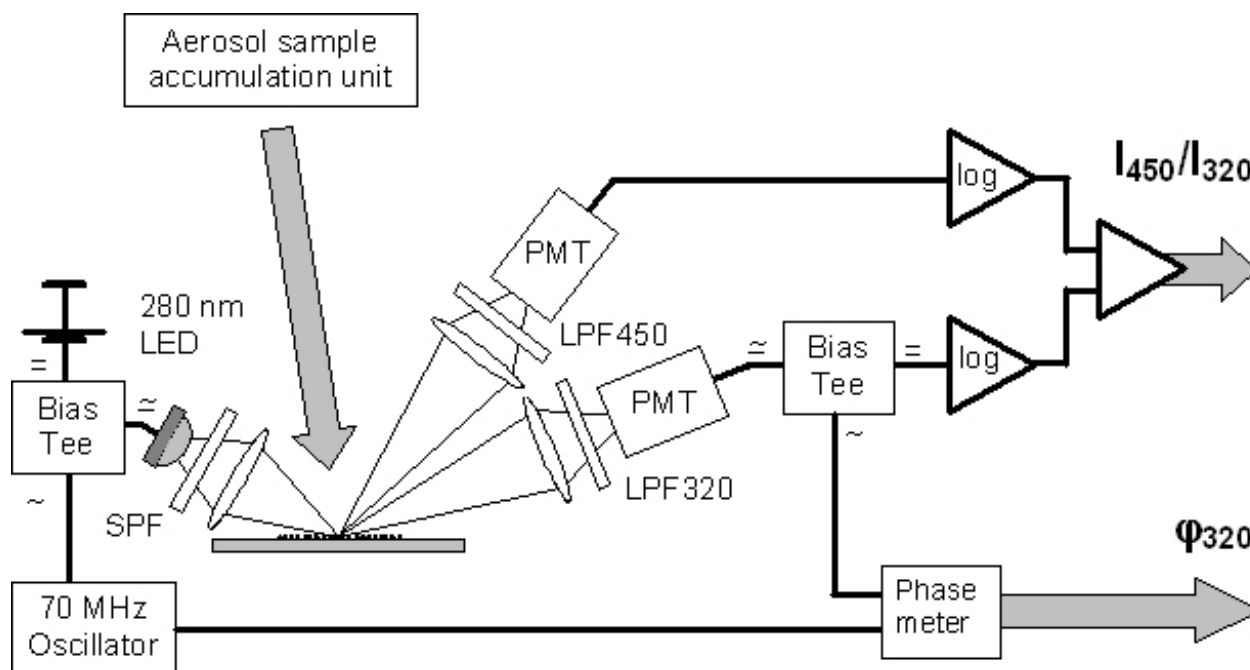


**Fig. 10.** Schematic presentation a proposed single-source biofluorescence sensor utilizing fluorescence spectral and phase signatures.

## 5. CONCLUSIONS

The analysis of the matrix of fluorescence spectral and phase signatures of *B. globigii* spores and common interferants under excitation by LEDs with different emission wavelengths enabled us to propose a new concept of a “detect-to-warn” biofluorescence sensor. In its simplest implementation, the sensor contains a single excitation source, 280-nm LED harmonically modulated at about 70 MHz frequency, and two photodetectors operating within the 320-nm and 450-nm spectral windows. The outputs of the sensor are the ratio of the fluorescence intensities in the two channels and the phase shift of the sinusoidal fluorescence waveform in respect of the excitation one in the 320-nm channel. In comparison with a conventional approach based just on the fluorescence intensity measurement, the concept fluorescence-phase sensor features a lower number of expensive optical elements and a potentially higher ability of discrimination of bioparticles against most common interferants (albuminous, epithelium, and cellulosous materials as well as aromatic hydrocarbons).

## ACKNOWLEDGEMENTS

The work was partially supported by the Lithuanian State Science and Studies Foundation under grant No C-18/2003. Effort was also sponsored by the Air Force Office of Scientific Research, Air Force Material Command, USAF, under grant number FA8655-06-1-3011. The U.S Government is authorized to reproduce and distribute reprints for Governmental purpose notwithstanding any copyright notation thereon.

## DISCLAIMER

The views and conclusions contained herein are those of the authors and should not be interpreted as necessarily representing the official policies or endorsements, either expressed or implied, of the Air Force Office of Scientific Research or the U.S. Government.

## REFERENCES

1. J. C. Carrano and A. J. Maltenfort, "Semiconductor ultraviolet sources for biological agent detection," *Proc. SPIE* **4743**, pp. 261–267, 2002.
2. P. Vitta, N. Kurilcik, A. Novickovas, S. Jursenas, H. Calkauskas, A. Zukauskas, and R. Gaska, "AlGaIn-based deep UV LEDs for fluorescence sensing," *Proc. SPIE* **5617**, pp. 249–260, 2004.
3. P. Vitta, N. Kurilcik, S. Juršėnas, A. Žukauskas, E. Bakienė, J. Zhang, T. Katona, Y. Bilenko, A. Lunev, X. Hu, J. Deng, and R. Gaska, "Fluorescence-lifetime identification of biological agents using deep ultraviolet light-emitting diodes," *Proc. SPIE* **5990**, pp. 0X1–0X14, 2005.
4. M. Wlodarski, K. Kwasny, and K. Kopczynski, "Stroboscopic technique for measurement of fluorescence lifetimes of bacteria and biological interferents," *Proc. SPIE* **6398**, 2006.
5. J. R. Lakowicz, *Principles of Fluorescence Spectroscopy*, Kluwer Academic/Plenum, New York, 1999.
6. M. A. Khan, M. Shatalov, H. P. Maruska, H. M. Wang, and E. Kuokstis, "III-Nitride UV devices," *Jpn. J. Appl. Phys.* **44**, pp. 7191–7206, 2005.
7. X. Hu, J. Deng, J. P. Zhang, A. Lunev, Y. Bilenko, T. Katona, M. S. Shur, R. Gaska, M. Shatalov, and M. A. Khan, "Deep ultraviolet light-emitting diodes," *Phys. Status Solidi A* **203**, pp. 1815–1818, 2006.
8. P. H. Kaye, E. Hirst, V. Foot, J. M. Clark, and K. Baxter, "A low-cost multi-channel aerosol fluorescence sensor for networked deployment," *Proc. SPIE* **5617**, pp. 388–398, 2004.
9. S. D. Campbell, D. P. Tremblay, F. Daver, and D. Cousins, "Multiwavelength bioaerosol sensor performance modeling," *Proc. SPIE* **5990**, pp. 0K1–0K13, 2005.
10. T. Pletcher, J. McGinn, D. Keller, A. Huston, J. Eversole, and V. Sivaprakasum, "Experimental performance of a novel aerosol sorting and deposition system for bio-treat sensing applications," *Proc. SPIE* **6398**, 2006.
11. P. Harms, J. Sipior, N. Ram, G. M. Carter, and G. Rao, "Low cost phase-modulation measurements of nanosecond fluorescence lifetimes using a lock-in amplifier," *Rev. Sci. Instrum.* **70**, pp. 1535–1539, 1999.
12. W. L. Nicholson and P. Setlow, "Sporulation, germination and out-growth," in *Molecular biological methods for Bacillus*, ed. by C. R. Harwood and S. M. Cutting, Wiley, Chichester, 1990, pp. 391–450.
13. T. J. Leighton and R. H. Doi, "The stability of messenger ribonucleic acid during sporulation in *Bacillus subtilis*," *J. Biol. Chem.* **246**, pp. 3189–3195, 1971.
14. J. Kunnil, S. Sarasanandarajah, E. Chacko, and L. Reinisch, "Effect of washing on identification of *Bacillus* spores by principal-component analysis of fluorescence data," *Appl. Optics* **45**, pp. 3659–3664, 2006.
15. A. S. Ladokhin, "Fluorescence spectroscopy in peptide and protein analysis," in *Encyclopedia of Analytical Chemistry*, ed. by R. A. Meyers, Wiley, Chichester, 2000, pp. 5762–5779.
16. K. Guzow, R. Ganzynkiewicz, A. Rzeska, J. Mrozek, M. Szabelski, J. Karolczak, A. Liwo, and W. Wiczak, "Photophysical properties of tyrosine and its simple derivatives studied by time-resolved fluorescence spectroscopy, global analysis, and theoretical calculations," *J. Phys. Chem. B* **108**, pp. 3879–3889, 2004.
17. R. Nudelman, B. V. Bronk, and S. Efrima "Fluorescence emission derived from dipicolinic acid, its sodium, and its calcium salts," *Appl. Spectrosc.* **54**, pp. 445–449, 2000.
18. *Handbook of Biomedical Fluorescence*, ed. By M.-A. Mycek, B. W. Pogue, Marcel Dekker, Inc., New York, 2003.

19. P. Vitta, N. Kurilčik, S. Juršėnas, A. Žukauskas, A. Lunev, Y. Bilenko, J. Zhang, X. Hu, J. Deng, T. Katona, and R. Gaska, "Deep-UV light-emitting diodes for frequency-domain measurements of fluorescence lifetime in basic biofluorophores," *Appl. Phys. Lett.* **87**, p. 084106–8, 2005.
20. A. P. Demchenko, *Ultraviolet Spectroscopy of Proteins*, Springer Verlag, New York, 1981.
21. J. A. Olmstead and D. G. Gray, "Fluorescence spectroscopy of cellulose, lignin, and mechanical pulps: A review," *J. Pulp Paper Sci.* **23**, pp. J571–J581, 1997.
22. Z. Deyl, K. Macek, M. Adam, and O. Vancikova, "Studies on the chemical nature of elastin fluorescence," *Biochim. Biophys. Acta.* **625**, pp. 248–541, 1980.
23. I. B. Berlman, *Handbook of fluorescence spectra of aromatic molecules*, Academic Press, London, 1971.